Research Article | Vol. 28, No. 2 / 20 January 2020 / Optics Express 1936
Optics EXPRESS

# Intracavity image upconversion system with fast and flexible electro-optic image gating based on polarization-frustrated phase-matching for range-gated applications

JUAN CAPMANY,* ADRIÁN J. TORREGROSA, AND HAROLDO MAESTRE

*Communications Engineering Department and I3E, Universidad Miguel Hernández de Elche. Avda. de la Universidad s/n, 03202 Elche, Spain*
*jcapmany@umh.es

**Abstract:** We report on a new image gating mechanism for intracavity nonlinear image upconversion systems that uses sum-frequency mixing of an external infrared image and a pump laser beam. Fast and flexible time duration gating of the upconverted image is achieved through transient electro-optic frustration of the phase-matching condition in a nonlinear crystal placed inside the cavity of the pump beam. The phase-matching condition is controlled by altering the polarization state of the laser cavity beam without interrupting laser oscillation, using a Pockels cell in one arm of an L-folded standing-wave resonator. In this way, an external image shutter mechanism is added to an image upconverter system that allows for using low shutter-speed EMCCDs (Electron Multiplying CCD) in range-gated imaging systems across the whole IR and potentially in the THz range.



## 1. Introduction

Range-gating is a useful technique to capture 2D (two-dimensional) images or video of objects submersed in scattering media like mist, smoke, fog, or sea-water [1], with potential for 3D (three-dimensional) reconstructions [2].

Due to the typical low energy exciting the sensor when a very short gating time is used in range-gated systems, it becomes advantageous to include a high luminance gain element like an image intensifier tube (IIT) with typical luminance gains ~$10^4$ or an ICCD camera (an IIT optically coupled to a CCD camera). Gating control in image intensifiers is easily achievable by reversing the bias of the photocathode, with a typical gating time capability ranging between ~ 3 ns and continuous operation of the intensifier. So far, this has been the choice in range-gated systems. Presently, new possibilities emerge with the advent of silicon electron multiplying CCD image sensors (EMCCDs), with an overall responsivity ~ $10^4$ - $10^5$ times that of a standard CCD, potentially reaching the single-photon detection level. EMCCDs have a lower signal-to-noise ratio (SNR) than ICCDs at low light levels, but also a lower price, higher resolution, longer operational life, and allow for higher mechanical shock resistant cameras. However, their main drawback is that although they include an electronic shutter, it is presently too slow for practical range-gating applications. Their typical shutter times are in the order 1-10 μs [3]. This represents a slice of distances in air around 300-3000 m, which makes them useless in most range-gating applications. Nevertheless, this problem could be overcome by adding an external fast image shutter device to the EMCCD.

The convenience of adding high gain in range-gated image systems imposes severe spectral limitations, due both to the photoemission cut-off wavelength of most photocathodes (typically multialcali or GaAs with $\lambda <$ ~ 900 nm [3]) and to the GAP of Si in EMCCDs $\lambda <$ ~1100

#383735 https://doi.org/10.1364/OE.383735
Journal © 2020 Received 20 Nov 2019; revised 2 Jan 2020; accepted 3 Jan 2020; published 14 Jan 2020

Optics EXPRESS

nm, both in the Visible/Near Infrared (VIS/NIR). There is, however, a present interest in the availability of range-gated systems in the infrared [4] such as in the eye-safe region around 1550 nm of the short-wave infrared (SWIR), or other spectral regions in the mid infrared (MIR) [5]. There, applications may benefit from an atmospheric transmission window around 3.3-4.1 μm [6], and from the weaker Rayleigh scattering than in the VIS/NIR. With the advent of nonlinear optics, the spectral limitations of Silicon Focal Plane Array (FPA) and ITT detectors can be overcome through nonlinear image upconversion based on nonlinear optical sum-frequency mixing (SFM) [7]. Recently, nonlinear upconversion of 2D images based on SFM, is proving a useful technique to overcome spectral, speed, and SNR limitations in 2D FPA-based GaAlAs and InSb cameras, or to avoid the significant cooling needs in infrared cameras by upconversion of the image to the NIR/VIS, and then detecting it with a Si-based FPA sensor [8–11]. In particular, intracavity continuous-wave (CW) systems like [8,9] are of great interest for boosting conversion efficiency, with image upconversion at the single-photon level having been already reported [11], and with a high potential of miniaturization [12]. Nonlinear image upconversion not only allows for image detection across the infrared, including mid and long IR wavelengths [13,14] or even the THz region [15], but as we show in this work, it also provides a natural mechanism for fast gating prior to detection. The mechanism is based on electro-optic temporal suppression of the image upconversion, which makes it useful as an external shutter for virtually any image sensor, including EMCCDs. As we discuss here, electro-optic image shutting, as obvious a resource it may seem, is by no means of straightforward appliance in (CW) intracavity image upconversion.

This work presents a technique to overcome simultaneously the spectral and gating-speed limitations of silicon EMCCDs, which will allow these sensors to be used in practical range-gated imaging systems virtually across the whole infrared, and potentially in the THz region. It relies on transiently frustrating a SFM-based intracavity image upconversion process, prior to entering the image sensor. The technique exploits the fast voltage-controlled electro-optic effect of an intracavity Pockels cell, acting on the polarization of a collimated fundamental (Gaussian) laser cavity beam that provides the pump wave for the SFM process, without interfering the incoming IR image.

In Section 2, we include a brief background of the range-gating technique. In Section 3, we summarize some basics of nonlinear image upconversion by SFM to understand the image resolution issues involved in our technique, which uses intracavity SFM. In Section 4, we analyze the possible use of an electro-optic image shutter in alternative configurations, and discard standard tentative (but not useful) configurations. In Section 5 we describe our experimental setup, and present and discuss our experimental results along with potential system instability issues. Finally, we present our conclusions in Section 6.

## 2. 2D range-gating background

In range-gating, a pulsed illumination source (usually a laser with a short pulse time duration $\tau_l$), is used to illuminate objects. A camera based on a 2D focal plane image sensor is time-gated, to allow the light reflected by the objects excite the sensor for only a short (gated) time interval. The time interval, determines a slice of distances reaching the image sensor of the camera (and thus being observed), on a time-of-flight basis. Any backscattered light or undesired reflections towards the camera originating out of the selected slice of distances is removed from the image reaching the sensor. This enhances notoriously the contrast of the objects in the image that would be obtained using continuous illumination. A schematic representation of a 2D full image range-gated system is represented in Fig. 1.

Gating consists usually of a given time delay $t_d$ (gating delay) between the illumination pulse emission and the enablement of the detector, and a second time interval $\tau_g$ (gating time) that corresponds to a time lapse in which the image is allowed into the detector. In general, short gating times in the order of the nanosecond and up to a few hundred nanoseconds are required

Optics EXPRESS

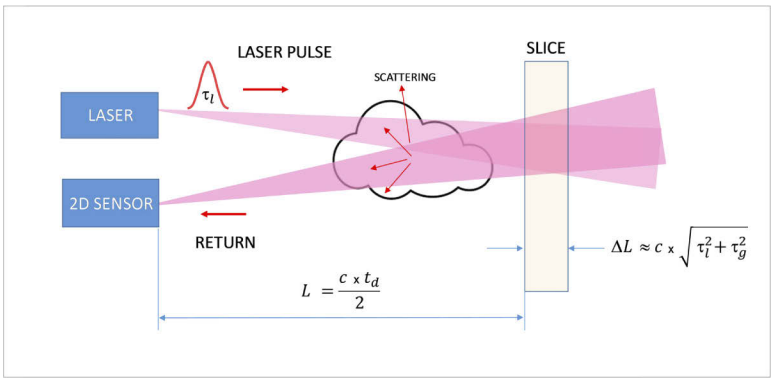


**Fig. 1.** Schematic representation of a 2D range-gated system showing the characteristic times and distances involved. The associated system optics and synchronism control are not shown.

for flexible outdoor observation of a thinner or wider slice of distances. Depth discrimination and 3D reconstruction depth resolution improve as the gating time reduces. For very short laser pulses compared to the gating time $\tau_l << \tau_g$, the distance slice width $\Delta L$ (Fig. 1) is determined only by the gating time $\Delta L \approx c\tau_g$.

## 3. CW intracavity image upconversion

The principle of SFM image upconversion taking place inside a nonlinear crystal is shown in Fig. 2(a).

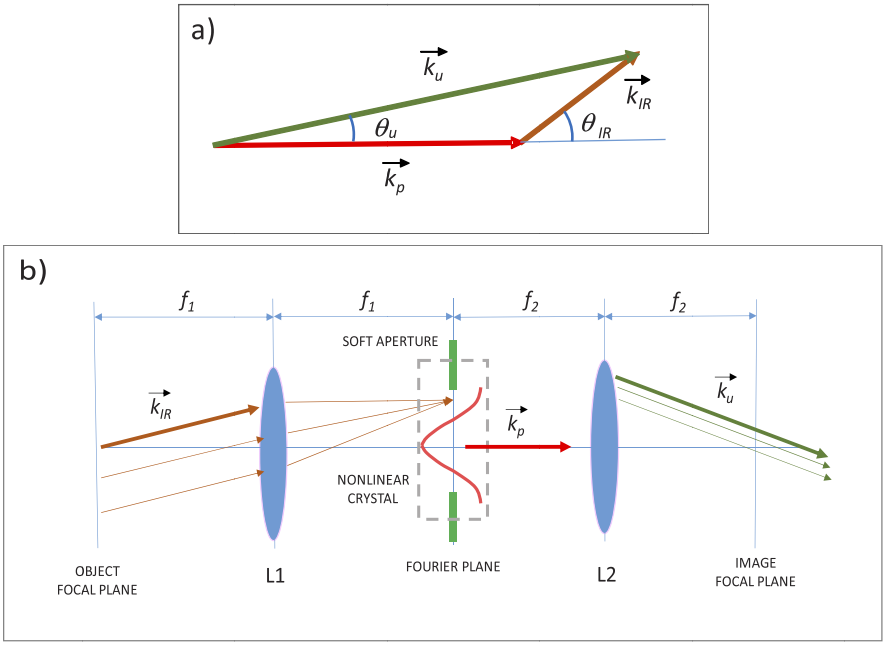


**Fig. 2.** a) Non-collinear SFM process inside the nonlinear crystal. b) The 4-f Fourier processor setup.

Optics EXPRESS

A Fourier plane-wave component in an 2D IR image, represented by a normal wave-vector $\vec{k}_{IR}$, is sum-frequency mixed (SFM) in a nonlinear crystal with a collimated (pump) laser beam, represented by a wave-vector $\vec{k}_p$, to produce a Fourier component of the upconverted image, represented by $\vec{k}_u$[16]. The total photon energy is conserved through the well-known relation $\omega_u = \omega_p + \omega_{IR}$, and a wavevector relation known as the phase-matching (PM) condition is required for efficient SFM: $\Delta\vec{k} = \vec{k}_u - (\vec{k}_p + \vec{k}_{IR}) \approx \vec{0}$ in birefringent or perfect phase-matching (BPM). Alternatively, in quasi-phase matching (QPM) $\Delta\vec{k} \approx \vec{G}$, where $\vec{G}$ denotes a reciprocal vector (or one of its harmonics) in a ferroelectric crystal having a spatial ferroelectric domain inversion distribution along the crystal. In order to upconvert a 2D image, non-collinear PM or QPM is required simultaneously for at least a range of $\theta_{IR}$ wavevector angles (normally forming a cone), contained within the Field of View (FOV) of the IR image. From the point of view of classical optics, image rays are required to propagate at different angles to the system optic axis, which direction will be taken as coincident with the pump laser propagation direction in what follows.

Typically, an image upconverter is built around a 4-f Fourier processor system (a telescope), with the center of the nonlinear crystal located in the Fourier plane of the 4-f setup as in Fig. 2(b).

The laser beam acts as a soft amplitude aperture in the Fourier plane, and sets a limit in the spatial frequencies (resolution) of the upconverted image. Regarding Fig. 2, we will need some results in our discussion that we establish here:

$$k_{IR} \sin\theta_{IR} = k_u \sin\theta_u \tag{1}$$

From Fourier Optics [17], the spatial frequency $\nu$ associated to a Fourier component of an image with wavenumber $k$ in a plane-wave expansion of the image is given by:

$$k \sin\theta = 2\pi\nu \tag{2}$$

where $\theta$ is the angle between the symmetry axis in a centered optical system and $k = nk_0$ the corresponding wavenumber in a medium of refractive index $n$ and vacuum wavelength $\lambda = 2\pi/k_0$. This is general, and holds for both images, infrared and upconverted. Thus:

$$\sin\theta_{IR} = \frac{1}{n_{IR}}\lambda_{IR}\nu_{IR} \tag{3}$$

$$\sin\theta_u = \frac{1}{n_u}\lambda_u\nu_u \tag{4}$$

and upconversion by SFM of a Fourier component preserves the spatial frequency inside the nonlinear crystal. By combining Eqs. (1), (3) and (4) inside the nonlinear crystal:

$$\frac{\nu_{IR}}{\nu_u} = 1 \tag{5}$$

However, because before and after the 4-f setup both infrared and upconverted images are in air, evaluating the real practical spatial frequencies requires accounting for the refraction in the air/nonlinear crystal interface. Then, introducing the Snell law in the air/crystal interface gives:

$$\frac{\nu_{IR}}{\nu_u} \times \frac{n_u}{n_{IR}} = 1 \approx \frac{\nu_{IR}}{\nu_u} \tag{6}$$

and thus, the spatial frequency is essentially conserved since $n_u \approx n_{IR}$. To our knowledge, this fact has not been discussed previously in the literature. It may also be pointed out, that the image

Optics EXPRESS

magnification of the 4-f setup with upconversion in the paraxial condition that follows from Fig. 2(a) is given by:

$$M_u \approx \frac{\lambda_u}{\lambda_{IR}} \times \left(-\frac{f_1}{f_2}\right) \tag{7}$$

As we will discuss later, PM angle acceptance limits the possible half-cone aperture angles $\theta_{IR}$ and $\theta_{up}$ from the optical symmetry axis to values not exceeding ≈ 100 - 200 mrad. Thus, image upconversion systems operate in the paraxial condition.

A final remark quantifying the effect on resolution of the soft aperture in the Fourier plane originating from a collimated Gaussian pump laser beam, is the intensity Point Spread Function (PSF) of the system, that can be approximately expressed as [8]:

$$PSF(r) \propto \exp\left(-\frac{\pi\,\omega\,r}{\lambda_u f_1}\right)^2 \tag{8}$$

where $r$ is the departure from the axis at the Fourier plane in the 4-f setup, and $\omega$ is the radius of the collimated pump laser Gaussian beam at $1/e^2$ intensity in the nonlinear crystal. Thus, tight focusing of the pump beam inside the nonlinear crystal reduces resolution, and it is more convenient to use a wider beam diameter in the pump beam. As a result, the pump beam will be in general a collimated beam inside the nonlinear crystal, with a large confocal parameter (Rayleigh range) that exceeds significantly the crystal length. The large beam diameter helps also in reducing the effect of spatial walk-off on the conversion efficiency. The conversion efficiency for a Fourier component, can thus be well approximated (neglecting loss) by an undepleted pump model that considers no Boyd-Kleinman focusing effects [18], and that for a Gaussian beam within regions close enough to the beam waist when compared to the confocal parameter (plane wave-front) is given by [8]:

$$I_u(x,y) = \frac{16\pi d_{eff}^2 \lambda_{IR}^2 l^2}{n_{IR} n_p n_u c \varepsilon_0 \lambda_u^4} \times \frac{f_1^2}{f_2^2} \times \frac{P_p}{\omega^2} \times I_{IR}(x',y') \tag{9}$$

where, $I_u\ (x,y)$ is the intensity of the upconverted image at the point $(x,y)$ in the image focal plane of lens L2. $I_{IR}\ (x',y')$ is the IR image intensity of a point located in the object focal plane of lens L1 with coordinates $x' = x/M_u$ and $y' = y/M_u$, accounting for the magnification factor $M_u$ defined in Eq. (7), $d_{eff}$ the effective second-order nonlinear coefficient of the crystal, $l$ the length of the crystal, $c$ and $\epsilon_0$ the speed of light and dielectric constant in vacuum respectively, and the rest of variables as defined previously.

We stress, that according to Eq. (9), conversion efficiency defined as $I_{up}\ /I_{IR}$, is proportional to the pump laser power density $P_p/\pi\omega^2$ inside the nonlinear crystal. Thus, the typical intracavity pump power density available in an intracavity conversion scheme, is advantageous for increasing conversion efficiency in the CW case, and in particular to compensate for the fact that pump power density reduces with large beam diameters. Intracavity CW conversion is very appealing, as it boosts nonlinear conversion efficiency, due to the high power density available in the laser mode that acts as the SFM pump laser beam in an intracavity nonlinear crystal. It also helps in decoupling the pump beam temporal structure in the upconversion process when using pulsed IR image illumination. As it was shown by R.G. Smith and co-workers [19], careful design can theoretically raise the conversion efficiency to a quantum efficiency QE ≈ 1, i.e., all incoming IR photons become upconverted. Although it was theoretically demonstrated and experimentally verified for second-harmonic generation (SHG) [20], there is no fundamental restriction in applying the same principles to SFM. However, this involves taking several aspects into consideration, including the length of the nonlinear crystal according to the intracavity power available. We have not pursued such an optimization here. Rather, the aim of this work is to propose and demonstrate a new kind of image shutter. In [8], for instance, a 20%

Optics EXPRESS

image upconversion efficiency in power is reported under non-optimized conditions. Intracavity upconversion takes place in the undepleted pump regime, thus preserving a linear relation between the relative intensity in the IR and the upconverted image points.

## 4. EO image gating alternative schemes

The fast response of the electro-optic (EO) effect seems attractive for building an image shutter for range-gating. In principle, a tentative resource could be EO blocking of the IR image before entering the upconversion system, and then transiently unblocking it. There are three possible EO-based image shutter schemes shown in Fig. 3, which include external (single-pass) and intracavity SFM. Although we analyze all these schemes in more detail later, we will show that only an intracavity scheme can achieve flexible gating time duration, a wide Field of View, and efficient upconversion altogether. In Fig. 3(a), we show a basic external conversion scheme. A combiner mixes the pump beam from an auxiliary laser and the IR image in a single-pass interaction through the nonlinear crystal. The IR image is focused inside the nonlinear crystal by a lens. A second lens retrieves the upconverted image and directs it towards the image sensor. An optical filter is added to block the remaining IR and pump laser powers, while letting only upconverted images through. Thus, impeding that an upconverted image develops and reaches the sensor through the filter, acts as an effective image shutter. The numbers in the figure indicate the possible locations for an upconversion-based EO external image shutter, consisting of a Pockels cell placed between crossed polarizers, to be used in later discussions. In Fig. 3(b), we show a typical intracavity conversion scheme where the nonlinear crystal is located inside the pump laser cavity.

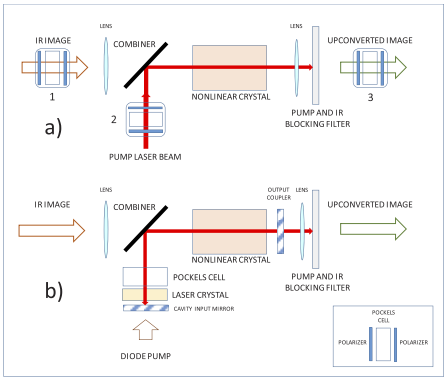


**Fig. 3.** Different EO image gating schemes. a) External, single-pass. b) Intracavity in an L-folded cavity.

In a first scheme, a natural way to proceed, is to place an electro-optic crystal (Pockels cell) between crossed linear polarizers, and make the IR image travel through the assembly (shutter) before reaching the upconverter (1 in Fig. 3(a)). This is valid for both intracavity and external upconversion. With a zero bias applied to the Pockels cell, the IR image is blocked by the crossed polarizers, and there would be no upconverted image. Because the assembly acts as a voltage-controlled shutter, transient application of a half-wave bias voltage to the cell would make the assembly let the IR image through, and produce an upconverted image for a desired gating time. We will refer to this unblocking situation as the ON state. A similar alternative scheme, also valid for the intracavity and external schemes, (3 in Fig. 3(a)) results if the shutter is located between the upconversion system and the detector. In this scheme, also valid both for external and intracavity upconversion, there is an effective image upconversion process, but its

Optics EXPRESS

way to the detector may be blocked by the shutter. As we analyze below, these schemes based on blocking an image, suffer from the interference issues in the upconverted image.

Another possible scheme, is to block the pump laser beam to avoid upconversion (2 in Fig. 3(a)). This is more convenient when the image upconversion takes place in a single-pass external nonlinear crystal. However, in case of using a CW pump laser beam, a high power beam would be required to make upconversion efficient, due to the convenience of using a large pump laser diameter for resolution issues. Using a pulsed pump laser beam from a Q-Switch or a mode-locked laser can increase conversion efficiency, but a very high pulse-repetition rate would be necessary for range-gating. A flexible gating time in the nanosecond range, requires the number of pulses in the ON state to change in not more than ~1 ns time increments, i.e., pulse repetition rates in the GHz range provided by an auxiliary Q-Switch or mode-locked laser. This scheme is thus not very practical for range-gating field equipment.

A fourth alternative, that we propose here, is to spoil or frustrate transiently the phase-matching requirement for efficient image upconversion, rather than blocking a beam or an image. This can be done by acting on the polarization state of the pump beam with an intracavity Pockels cell, and no additional polarizers. As we show later, this last technique can be applied to intracavity upconversion in a CW laser. Applying this technique to an external conversion scheme does not help in overcoming the efficiency or pulse repetition frequency issues already described. Thus, we concentrate on schemes potentially valid for the intracavity case, and analyze them in more detail next. It should be emphasized, that intracavity blocking of the pump beam is not a valid solution, because the onset of Q-Switch pulses must be avoided. A Q-Switch pulse has a well-defined duration time in a laser, and its duration cannot be significantly altered, thus impeding a flexible gating time.

### 4.1. Direct EO shuttering of the IR image or the upconverted image

Because high performance range-gated systems use laser illumination with a relatively narrowband bandwidth, the different optical paths that undergo the different IR image rays inside the electro-optic crystal, leave obscure rings in the IR image to be upconverted when the Pockels cell is placed between the crossed polarizers (conoscopic interference patterns in a polariscope [21,22]). These patterns, that are bias-dependent, convolve with the IR image, and would then appear in the upconverted image as well. The effect is illustrated in Fig. 4, and takes place in Pockels cells situated between crossed polarizers. For a uniaxial crystal like KD*P, the conoscopic interference pattern for rays propagating close to the optical axis is determined by [22]:

$$\frac{I_2}{I_1} = \sin^2(2\alpha) \times \sin^2\left[\frac{\pi}{\lambda}\Delta n\,(V) \times L\right] \tag{10}$$

where $I_2$ and $I_1$ are the point intensities with and without interference, respectively, and $\Delta n(V)$ represents the birefringence index ($n_o$-$n_e$), that changes with the Pockels cell bias voltage $V$. $L$ and $\alpha$ are the polar coordinates shown in Fig. 4(a).

However, the effect takes place also in Pockels cells with the transversal configuration (transversal biasing). For large aperture Pockels cells, it is convenient to use a longitudinal Pockels cell, with a longitudinal field applied to the uniaxial crystal, i.e., a longitudinal biasing. In case of a longitudinal KD*P Pockels cell, the induced principal axes occur at $\alpha = \pm 45°$ for an electric field applied along the Z-axis [23]. The same effect is expected if the upconverted image is passed through the Pockels cell shutter as in location 3 in Fig. 3(a).

Recently, an attempt of such a general-purpose (with no upconversion) image shutter has been investigated, by restricting image ray angles to a small region around the axis, after choosing a suitable Pockels cell voltage to optimize the aperture within the conoscopic interference pattern [24], as shown by the circle or alternatively the rectangle in Fig. 4(b)). However, this small region around the axis can only provide a FOV (full cone angle) of 0.9 mrad (a half cone angle of

Optics EXPRESS

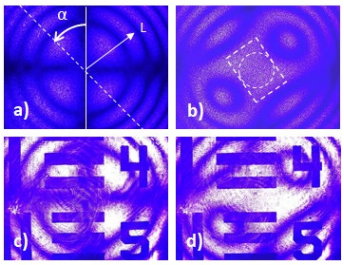


**Fig. 4.** Conoscopic interference patterns realized with a 405 nm laser to show the effect. a) without biasing the Pockels cell. b) with biasing optimized to leave a useful aperture close to the center of the pattern. c) and d) are the same as a) and b), but convolved with a target image before traversing the Pockels cell shutter.

0.029°) where the full image has to be constrained. Such a limitation is too detrimental for the resolution of the system.

The highest spatial frequencies contained in the image are given by (2). Thus, wide angle apertures are beneficial for resolution. For instance, in an eye-safe image around $\lambda$=1550 nm in an $n = 1.5$ crystal, a 0.9 mrad FOV would set a resolution limit of $\nu \sim 1$ lp/mm in the object focal plane of the system. However, an intracavity upconversion system where a $\lambda$=1550 nm image mixes with a pump laser beam of 1064 nm and a beam diameter 0.8 mm, has the capability of reaching typically $\nu \sim 60$ lp/mm for a 25 mm focal length lens in the input of the 4-f system (set by laser beam diameter). This is comparable to the typical resolution of ICCDs (usually set by the output tapered fiber bundle of ITTs used for image coupling to a CCD sensor). Yet, a limitation may be imposed by QPM or PM tolerances. Typical tolerances exploiting tangential BPM for monochromatic interactions can be in the order of 0.13 rad (half cone angle) [25], that sets a resolution limit around 125 lp/mm. However, there are PM angular-acceptance increasing techniques, like using a wider spectral width in either the laser beam or the IR illumination [9,10], chirping the nonlinear crystal domains in QPM or introducing a temperature gradient in it [26], or using adiabatic SFM as in [27]. Thus, a resolution limit set by the soft aperture that the laser beam diameter represents, is reasonably in the order of 50-60 lp/mm at the focal plane of L1, although it can be improved.

It should be pointed out, that trying to rotate the IR image polarization with a Pockels cell prior to entering the upconversion system in the absence of any additional polarizer, leads also to a conoscopic interference in the upconverted image. We have checked this circumstance experimentally. The effect is weaker, but it is still there. We believe it takes place because the fact that PM for upconversion requires projection of the IR image polarization over a specific nonlinear crystal axis, makes SFM behave as an effective polarizer added to the incoming polarized IR image.

### *4.2. Gating by upconversion frustration through polarization control*

Due to the limitations discussed about EO blocking the IR image, we propose a more efficient way of exploiting the high speed of the EO effect for gating in image upconversion systems. Rather than transiently blocking the IR image or pump laser passage to the nonlinear crystal, our proposal is to control the image upconversion time by electro-optically frustrating the PM condition, and then restoring it for a short interval of time. One way to do it, is by designing a cavity where the laser beam polarization can be altered (rotated 90°) in the ON/OFF states, without interrupting the laser oscillation in order to avoid reaching the Q-Switch regime. Because

Optics EXPRESS

PM requires a specific pump beam polarization for efficient SFM, this technique inhibits/enables image upconversion during a time interval.

One of the requisites for nonlinear upconversion, is that the polarization of the mixing waves satisfy the wavevector relation in SFM. In Type 0 QPM (e + e → e) and Type I BPM (e + e → o or o + o → e), the laser and the IR image must be of the same polarization, whereas in Type II BPM they need to be of orthogonal polarization (o + e → e, o + e → o, e + o → e, or e + o → o) [28]. Regardless the Type of BPM or QPM, once a crystal is prepared for a nonlinear interaction at a suitable propagation angle, if the pump wave polarization is rotated 90°, the nonlinear interaction efficiency vanishes and there is no resulting upconversion. If conoscopic interference patterns are to be avoided, no passage of any polarized image can be allowed through the Pockels cell, which can be easily realized using an L-folded cavity like in Fig. 3(b), and inserting a Pockels cell in one cavity arm, with no additional polarizers. It should be noted, that the addition of the Pockels cell in this way, introduces no additional limitation in FOV, conversion efficiency, signal-to-noise, or resolution, to those inherent in nonlinear image upconversion. We have used this technique, and describe our results next.

## 5. Experimental setup

The complete experimental setup used (except for the CCD camera), is schematically shown in Fig. 5. We have used a 1064 nm laser to upconvert 1342 nm images to 593 nm (yellow) for demonstration purposes, due to our experimental convenience in using the available resources in our laboratory. It can be easily understood that it is possible to work at other IR spectral regions by a suitable choice of the laser + nonlinear crystal combination, as long as the sum-frequency falls within spectral response range of the camera sensor, and that our proposal is of general application.

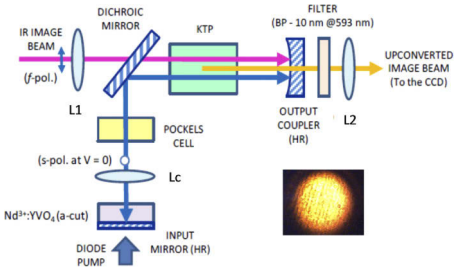


**Fig. 5.** Schematic representation of the complete image upconversion experimental setup. The CCD camera is not represented. The inset shows an upconverted image of the IR illumination beam with no target. The distortions observed in the upconverted image are due to malfunction of our yellow band-pass filter.

For illumination, we have used a CW linearly polarized 1342 nm laser based on an a-cut $YVO_4$:$Nd^{3+}$ laser crystal. The laser is diode end-pumped at 808 nm. The intracavity CW pump wave for SFM at 1064 nm is based also on an a-cut $YVO_4$:$Nd^{3+}$ laser crystal. The cavity is a standing-wave resonator with a dichroic mirror (beam combiner) used to form a 90° L-folded cavity with a total length of 30 cm. One of the cavity mirrors (input mirror) has an HR dielectric coating deposited on the laser crystal, and the output coupler is a concave 3 mm radius of curvature (ROC) mirror with a nominal reflectance of 99.95%. The laser crystal has a cross sectional area of $3 \times 3$ mm$^2$ and a length of 4 mm, and is AR coated at 1064 nm on the cavity side. A KD*P longitudinal Pockels cell (9 mm diameter aperture, 30 mm long) is inserted in the laser crystal cavity arm, after a positive lens ($L_c$) of 50 mm focal length, and before the dichroic mirror.

Optics EXPRESS

Regarding the KTP crystal used, it was an $8 \times 8 \times 10$ mm$^3$ crystal, initially cut at $\theta = 60°$, $\varphi = 0°$ (X-Z crystal principal plane, $d_{eff} = 3.2$ pm/V), for Type II SHG of 1342 nm, with AR coating optimized for the fundamental wave and the second harmonic. However, this orientation is only 1.5° (internal angle) away from the right direction required for 1064(e) + 1342(o) nm → 593(o) nm SFM, so it was used with a slight misalignment with respect to the cavity symmetry axis. The theoretical internal PM acceptance angle is 1.36 mrad × cm, i.e, 1.36 mrad in our case, 2.38 mrad for external rays due to the ~ 1.75 refractive index of KTP. Tangential phase-matching [24] was not pursued here. The KTP crystal (positive birefringence) is oriented with its slow polarization axis (*s-pol*) perpendicular to the plane of Fig. 5, and its fast polarization axis (*f-pol*) in the plane of the figure.

Yellow upconverted images start to be discernible with the camera for an illumination of only 200 μW CW power at 1342 nm incident on a transmission target located at the object focal plane of L1, and a diode-pump emission power of only 1 W at 808 nm.

### 5.1. The cavity design

The cavity design we have used has several useful characteristics. It is a standing-wave L-folded cavity with an intracavity convergent lens, closed by a flat input mirror and an almost-flat output coupler, both of very high reflectance at the oscillation wavelength. Folding is achieved by a flat-flat dichroic beam combiner mirror, with very highly reflection at the oscillation wavelength, and very high transmission for the IR image. One cavity arm accommodates the laser crystal, the lens and the Pockels cell. The other arm accommodates only the nonlinear crystal. This allows passing the IR image straight through the nonlinear crystal, traversing only the flat-flat beam (combiner), just by adding the lenses of the image forming 4-f optical system, and avoids passing the image through the Pockels cell. The output coupler has a large radius of curvature to introduce negligible aberration in the image, while helping to keep the fundamental mode diameter stable. Because the L-folding beam combiner is flat and tilted 45°, it does not affect modeling of the cavity stability margin and mode size, which are set by the total cavity length. The fundamental mode profile is shown in Fig. 6.

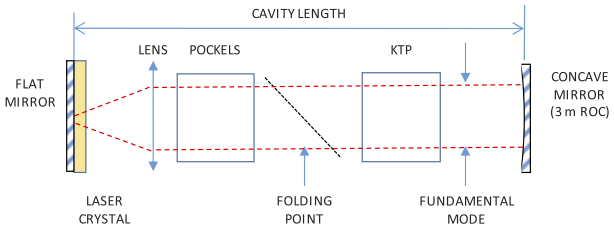


**Fig. 6.** Fundamental mode profile in the cavity (red dotted lines).

The inclusion of the convergent lens has several purposes. It was included to define a collimated Gaussian beam though the nonlinear crystal with variable diameter, to expand and collimate the beam in its passage through the Pockels cell, and to keep a tight focusing in the laser crystal, not to produce a threshold increase associated to a large mode diameter in the gain medium.

In our experimental conditions, the total cavity length is 30 cm, the fundamental mode diameter behind the lens is 0.92 mm, with $L_c$ located at a distance of 50.3 mm from the input mirror. The mode beam waist that takes place on the flat mirror deposited on the gain crystal is 37 μm. The cavity results stable for total cavity lengths larger than ~ 117 mm. Thermal lensing effects have not been considered in the design. The soft aperture resolution limit calculated for our 50 mm focal input lens L1 is 35 lp/mm, that corresponds to group 5 element 2 in a 1951 USAF resolution target located in the object focal plane of L1 (Fig. 5). It should be noted that the mode

Optics EXPRESS

beam radius is sensitive to slight variation in the lens position relative to the input mirror. For a distance of 52.9 mm to the input mirror, the beam diameter is 1.7 mm, and reduces progressively with increasing lens distance, reaching 0.66 mm for 55.0 mm with the cavity length set to 30 cm. Thus, there is large flexibility in adjusting the fundamental mode size. One can check the great flexibility in conforming the fundamental mode in this cavity design through the two degrees of freedom (lens position and cavity length), by using the cavity modelling free software provided in [29], which we have used throughout our design. The cavity also results stable in a wide range of lengths if the concave mirror is replaced by a flat mirror.

### 5.2. Intracavity polarization rotation in CW

A theoretical analysis of the polarization eigenmodes, can be done based on the Jones Matrices formalism in a way similar to [30], although it becomes more complex here, as we include a longitudinal KD*P Pockels cell with variable bias. Our interest focuses on the polarization state of the cavity beam just prior to entering the KTP crystal, in order to control PM frustration through polarization state control.

The theoretical analysis becomes cumbersome and extensive to be included in this work, and we merely present the model behavior in our experimental conditions, along with the experimental data measured. The system has two linearly polarized eigenmodes $s$ and $f$ (vertical and horizontal, respectively). These eigenmodes take place when the biases applied to the Pockels cell are zero and the half-wave voltage, respectively. For intermediate values of the bias, the polarization in the cavity undergoes arbitrary elliptical polarization states. Theoretically, when there are no polarization dependent gain/losses in the cavity, the total laser power remains constant at any arbitrary polarization state, and there is a full 90° rotation of the polarization when switching between the unbiased Pockels cell and the half-wave voltage. However, when there are intracavity elements with polarization dependent loss, the situation changes, and the laser power does not remain constant for different voltages applied to the Pockels cell. Instead, modelling predicts that there is a smooth variation in the total laser power. Typically, practical dielectric coatings on tilted surfaces behave slightly different in distinct polarizations. In particular, our dichroic combiner has nominal polarization reflection coefficients R = 98.72% (p-pol = *f-pol*) and R = 99.79% (s-pol = *s-pol*) for a fundamental wavelength of 1064 nm. This may not seem a significant polarization loss difference, but indeed has a noticeable influence in the laser power behavior because our cavity input and output mirrors have both nominal reflectances in excess of 99.5%. Thus, our cavity presents a high finesse in the vertical polarization and a lower one in the horizontal polarization. When the Pockels cell is unbiased, the polarization state in the combiner mirror is vertical (s-pol). When voltages other than zero are applied to the cell, a horizontal component develops in the combiner, which increases cavity loss, with the highest loss occurring when all the laser power in the combiner is in the horizontal polarization. Figure 7 shows the theoretical/experimental behavior when polarization dependent losses are included in a cavity roundtrip.

The theoretical value represented, is the normalized transmittance (total cavity loss) at different biases of the cell, computed in our estimated polarization-dependent loss conditions. The experimental values, are also normalized values of the laser power, measured in the vertical and horizontal polarizations behind the output coupler as the bias voltage of the Pockels cell changes (Figs. 7(a) and 7(b)). It can be seen, that there is a laser power continuous variation with static cell bias in our system. It should be noted, however, that such variation in power can be allowed, as long as oscillation does not stop, thus setting a favourable condition for creating a giant a Q-Switch pulse during fast changes in the Pockels cell bias. This continuous variation is not important for range-gating, as range-gating switches between two ON/OFF states, and the laser power available in the OFF state is unimportant, as long as such residual power is in the non-upconverting polarization. The important feature here, is that laser oscillation does not

Optics EXPRESS

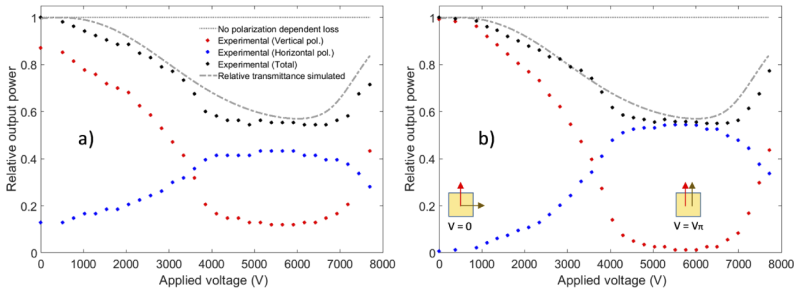


**Fig. 7.** a) Relative output laser power in the vertical and horizontal polarizations, total (added) laser output power, and simulated total roundtrip cavity relative transmittance with (curved) and without (flat line) intracavity polarization-dependent loss. The ~ 8:1 low polarization extinction ratio is due to a slight orientation misalignment in the s and f polarization axes of KTP with respect to the vertical in Fig. 5. b) Same as a), but with fine adjustment of the KTP crystal orientation. The polarization extinction ratio increases up to ~ 100:1. The insets in b) represent the KTP crystal cross sectional area, with the brown and red arrows indicating the polarization direction of the IR image and pump beam respectively, for 0 and half-wave voltages in the Pockels cell.

extinguish at any bias point of the Pockels cell. However, as we will analyze later, this leads to a gain/loss modulation in the laser when switching the bias value of the Pockels cell.

Figure 7(a) represents the situation when there is some misalignment among the polarization axes of the intracavity elements. As seen, the contrast ratio in the ON/OFF situations degrade. This contrast ratio is around 8:1 in Fig. 7(a). However, with fine orientation alignment following a procedure such as that described in Section 5.4, the power in one of the polarization components can be set virtually to zero in the OFF state, thus leading to a very high contrast ratio (virtually infinite, in practice to the typical extinction ratios of 100:1 or more in real polarizing elements). A similar situation with a precise experimental verification is discussed in [12].

In Fig. 8, we show the upconverted image intensity at various voltages applied to the Pockels cell. The small spots observed in the yellow regions are due to our defective yellow interference filter. The image shown corresponds to group 4, elements 5 and 6 in the target. The upconverted image diameter corresponds to 0.22 mm in the object focal plane of L1 ($f_1 = 50$ mm), which gives an upconverted FOV (half cone angle) of 2.2 mrad (0.14°). This FOV is limited by PM angle acceptance, and can be significantly improved by more than one order of magnitude using tangential PM. Although we did not pursue this optimization here, this FOV value is already ~ 5 times larger than that reported in [24].

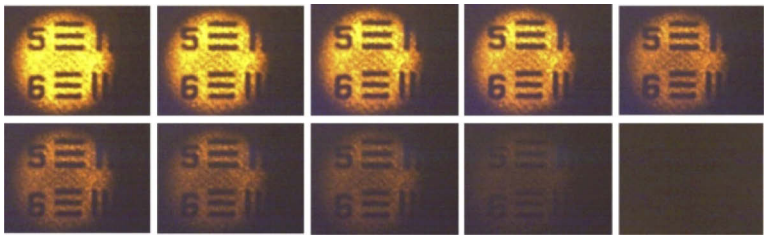

**Fig. 8.** Upconverted image for increased static biasing of the Pockels cell, from top to bottom and left to right. Top left corresponds to V = 0 V. Bottom right corresponds to upconverted image full extinction, which takes place at V ~5.5 kV, near the 6 kV nominal half-wave voltage of the cell.

Optics EXPRESS

### 5.3. Fast gating

Due to the variation in laser power with the bias voltage applied to the Pockels cell, a periodic switching between the ON/OFF states of the upconverted image, introduces a periodic modulation in the gain/loss. This results in dynamical processes in the laser, which can be inherited by the upconverted image, leading even to potential laser instability. Before analyzing the possible dynamical processes in the laser, we must note that Figs. 7(a) and 7(b) were measured through slow changes in the Pockels cell bias. For fast EO alteration of the Pockels cell refractive indices, one could tentatively think that some of the axial modes in the standing-wave cavity, may violate transiently the resonance condition due to a variation in the optical path of the cavity, and that it would take some time for them to ring down, and for other new oscillation modes to build up, then creating conditions for building up a Q-Switch pulse. Rather, the index change produced by the intracavity Pockels cell, introduces a fast phase modulation on the oscillation modes, which can be physically interpreted as an instantaneous Doppler frequency shift [31]. Because the fast variation in index resembles a linear change, the analysis is quite close to that of a fast intracavity linear phase modulation. In essence, oscillation does not stop at any time while fastly changing the bias of the Pockels cell. Thus, there is no chance for creating a population inversion above threshold that can result in building up a Q-Switch pulse. This is in agreement with the experimental transient behavior shown in Fig. 9. Once we have shown that discontinuity in laser oscillation with varying Pockels cell bias does not take place, the most likely and important dynamical effects to be considered here, are the possibility of mode-locking, self-pulsing, large amplitude fluctuations by the intracavity nonlinear interactions [32,33], and the natural occurrence of relaxation oscillations in solid-state lasers (SSL). We analyze them next.

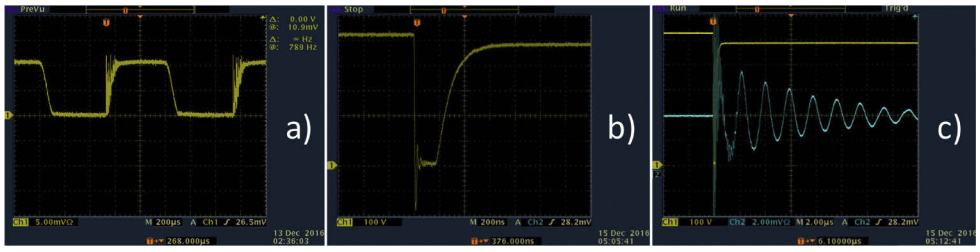


**Fig. 9.** a) Upconverted signal for a periodic bias of the Pockels cell. b) Electric pulse applied to the Pockels cell. c) Pockels cell bias (yellow trace using a 1:10 probe divider) and transient photocurrent in the photodetector (blue trace, AC coupled to the oscilloscope) showing the relaxation oscillations in the upconverted wavelength.

#### 5.3.1. Mode-locking

Mode locking requires that the axial mode spacing of the standing-wave cavity is matched to the frequency or higher harmonics of the gain/loss modulation fundamental frequency. The estimation for an empty standing-wave cavity, with an axial mode spacing of $\Delta\nu = c/2L$, gives an axial mode spacing of at least 300 MHz, for a cavity not longer than 50 cm. Thus, there is a wide margin for practical SSL design, where mode-locking would not be present at practical range-gating pulse repetition frequencies, that are typically not higher than 10 kHz, and in many cases around 50-60 Hz.

#### 5.3.2. Nonlinear cavity dynamical effects

The other phenomena, periodic or chaotic self-pulsing, and large amplitude fluctuations due to intracavity nonlinear interaction among axial modes [32,33], are more difficult to estimate. But in essence, because the IR image is an external wave, the nonlinear energy exchange mechanism

Optics EXPRESS

among the laser axial modes requires PM around the SHG condition, or cascaded $\chi^{(2)}$ SFM:DFG processes that are of a much weaker strength. Antiphase Dynamics leading to individual axial mode amplitude fluctuations is neither expected to play any significant role. Firstly, because of the time scale compared with the frame integration time of the image sensor, and secondly because in Antiphase Dynamics, the total power remains essentially constant despite the individual mode fluctuations. This situation requires the absence of mode partition noise [34] in the upconverted image, which is absent due to the relatively wide wavelength acceptance for SFM. The PM wavelength acceptance tolerance, permits that any of the potential oscillation modes lead to efficient SFM. The acceptance bandwidths for 1342 and 1064 nm SFM in our 1 cm KTP are 10.86 and 52.55 $cm^{-1}$ [35]. This represents a wavelength tolerance for 1064 nm of ~ 5 nm, wide enough to accommodate all the possible oscillation modes within the gain linewidth of the a-cut $YVO_4$:$Nd^{3+}$ crystal, which room temperature $\pi$-polarized emission cross section linewidth in the 1064 nm transition (9397.7 $cm^{-1}$) is 6.9 $cm^{-1}$ (0.96 nm) [36]. We have experimentally checked the absence of these effects in our system. It should be noted, that were this a problem, there is always the possibility of using a unidirectional single-axial mode cavity configuration to avoid axial mode competition [33].

In essence, there are no dynamical instabilities caused by the intracavity upconverted image-frustration process. To be complete, also, the pump requirements in possible upconversion systems are largely below the "second threshold" for chaos in C-Class solid-state lasers [32].

#### 5.3.3. Relaxation oscillations

Periodic modulation of the gain/loss, however, leads to the appearance of relaxation oscillations (RO) in SSL. This would not represent a limitation in semiconductor lasers as it is a fast transient effect in the GHz regime, which is not relevant as it is averaged by the frame integration time of FPA sensors. However, RO frequencies in SSL are lower than in diode lasers, and it becomes an issue, as gating time control for times below the duration of a single RO becomes challenging. There are examples of gain switched laser systems reported to allow for only one RO [37].

In our setup, built around a high finesse cavity, as demanded by efficient intracavity upconversion, the period of the relaxation oscillations is ~ 2 µs. Figure 9(a) shows the upconverted intensity in our system when a periodic bias is applied to the Pockels cell. The RO can be clearly appreciated.

Figure 9(b) shows the temporal behavior of an electric voltage pulse of ~ 5.5 kV applied to the Pockels cell. Figure 9(c) shows the transient current response of the yellow upconverted power in the detector, measured with a 100 MHz bandwidth oscilloscope and a 455 ns rise time detector, where the RO are displayed in more detail, and where oscillation in the fundamental mode alone is forced with an intracavity pinhole. Due to the HV switch used, bias pulses shorter than below 200 ns could not be applied to the Pockels cell.

To be useful in practical range-gated systems that can gate down to a few nanoseconds, the system requires that the RO are removed, or at least highly attenuated. At difference with most gas lasers, the occurrence of relaxation oscillations is a natural effect in solid-state lasers. The most natural way to avoid RO in SSL, would be to design the cavity with optical elements so that there are no polarization-dependent gain/losses at any bias of the Pockels cell. This includes taking into consideration that gain may take place in only one polarization as in case of using an a-cut $YVO_4$:$Nd^{3+}$ crystal like we do. The situation is similar if an isotropic crystal like $Nd^{3+}$:YAG is used in conjunction with an intracavity Brewster plate. We do not attempt to damp the RO it in this work, and we are presently carrying out an investigation of whether the cavity gain/loss can be made independent of the polarization at all. However, because there is another degree of freedom in controlling the intracavity power in diode-pumped solid-state lasers through variation of the diode pump power, RO can be eliminated, or at least heavily attenuated, by use of electronic feedback on the diode pump power [38], or by adding a pre-distortion compensating current pulse to the pump current [39]. An improved cavity design with balanced loss/gain at

Optics EXPRESS

both eigenpolarizations, could presumably help in further attenuation of the RO with these two techniques. We leave this problem for future investigation, although we describe a balanced polarization-loss scheme in Fig. 10. Here, we show that integration of an EO fast image gating control is possible in intracavity SFM, without inducing Q-Switch pulses, and that the intracavity PM control through polarization control of the SFM pump laser we describe, introduces no conoscopic interference patterns in the upconverted image. Destroying PM by EO detuning of angle/spectral tolerance is not feasible, because good resolution requires wide angle/wavelength acceptance, which is difficult to fully detune electro-optically.

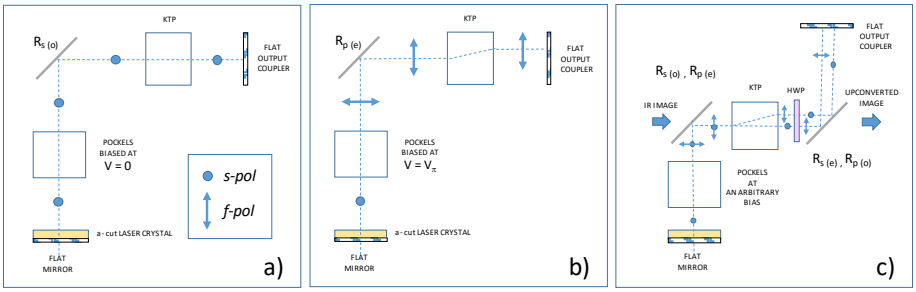


**Fig. 10.** a) Cavity roundtrip path with only one combiner for a) V = 0 and b) $V = V_\pi$ applied to the Pockels cell. In c), a polarization independent loss configuration is shown, using two similiar commerical dichroic combiners, and adding a half-wave plate (HWP).

### *5.4. Pockels cell operational life, fine polarization alignment, and balancing polarization-dependent cavity loss*

In general, it is not convenient to keep biased some widespread longitudinal Pockels cells like KD*P for long times, as it shortens its useful life. Periodic gating in the nanosecond regime, requires in general a very small duty cycle, even at repetition frequencies of 100 kHz ($D = 10^{-4}$ in this case). Thus, for EO gating, it would be better to start with the wrong (non-upconverting) polarization in the laser, and then rotate it for a short interval of time by applying a short time bias pulse to the Pockels cell. Then, during most of the time in a cycle, there is no upconversion. Without entering electronic discussions that are beyond the scope of this work, we have used the discharge of a capacitor previously charged at a high voltage (HV). The capacitor is charged by a HV power supply, and then discharged with a HV MOSFET switch. Unfortunately, our HV switch (Behlke 80-HTS) can only produce fix duration pulses not shorter than 50 ns when optimized. In fact, the electric current pulse overshot in Fig. 9(b), shows unmatched impedances and bad electric pulse dumping in our case, and a pulse duration around 200 ns. There are, however, faster and flexible duration HV pulsers commercially available.

In addition, when starting with the non-upconverting polarization, a fine orientation alignment of the birefringent KTP is easier to realize, in order to remove any undesired trace of the upconverting orthogonal polarization component. By checking the polarization state and the presence of any residual upconverted power, the contrast image ON/OFF ratio can be maximized, and indeed set to a very high value.

Commercial dichroic beam splitters/combiners usually present a different reflectance $R_s$ and $R_p$ in s and p polarizations. To avoid the special design of a dichroic combiner to balance loss in both polarizations, a scheme like the one in Fig. 10(c) can be followed. It is based on using two identical (or very similar) intracavity dichroic combiners, where their s and p polarizations are swapped for the ordinary (o) and extraordinary (e) waves in a second combiner by inserting a

Optics EXPRESS

half-wave plate, i.e., if $R_o = R_s$ and $R_e = R_p$ in first combiner, $R_o = R_p$ and $R_e = R_s$ in the second one.

Regarding spatial walk-off associated to double refraction in a critical PM situation, a tandem or twin-crystal compensating configuration in the KTP crystal, can be used as in [40] if desired. We assume no walk-off in the Pockels cell, as it is used in a longitudinal configuration, with both polarizations propagating along a principal crystal axis (Z). Assuming then, that the only (or main) polarization-dependent loss in the cavity arises from the dichroic combiner, we see that in the configuration of Fig. 10(c), the roundtrip loss factor for both polarizations is $L = 1 - R_s^2 R_p^2$.

## 6. Conclusion

An electro-optic gating control has been integrated in a CW intracavity image upconversion system. The system acts simultaneously as an IR image upconverter to the visible, and as a fast image shutter of the upconverted image. This allows EMCCDs to be used as image detectors in range-gated applications in the infrared, by providing a spectral shift from the IR to the sensor spectral response, and by providing an external shutter mechanism that operates faster than the electronic shutter of the EMCCD. We have shown, that due to the appearance of conoscopic interference, electro-optically blocking the IR image before entering the upconversion system, is not a satisfactory solution in laser illuminated range-gating systems. Our proposal, is based on transiently frustrating the PM condition in an intracavity SFM process, by rotating the polarization of the intracavity Gaussian pump beam. We use an L-folded cavity with a Pockels cell placed in one arm of the cavity, and the nonlinear crystal placed in the other arm. During electro-optic intracavity polarization rotation of the laser beam, laser oscillation does not stop at any time. This avoids the build-up of a Q-Switch pulse that would impede adjusting a flexible gating time duration. The technique introduces no conoscopic interference in the upconverted image. This technique can also be used with poled nonlinear ferroelectric crystals like PPLN or PPKTP, by replacing our birefringent nonlinear crystal with a poled crystal providing QPM. The most efficient QPM is Type 0 QPM, where all waves are linearly polarized parallel to the ferroelectric c-axis (extraordinary waves), i.e., an e(IR) +e(p) $\rightarrow$ e(u) interaction. Rotation of the pump beam polarization would result in a e(IR) +o(p) $\rightarrow$ e(u) interaction, which frustrates the Type 0 QPM condition.

In our work, we have used a 1064 nm $YVO_4$:$Nd^{3+}$ laser to upconvert 1342 nm images to 593 nm in a KTP crystal for demonstration purposes, using the resources available in our laboratory. It can be easily understood, that it is possible to work with images in other IR spectral regions, and potentially in the THz region, by a suitable choice of the laser and nonlinear crystal combination, as long as the sum-frequency wavelength falls within the spectral response range of the camera sensor, and as long as a suitable Pockels cell material is available.

In a step forward in integration, the Pockels cell may perhaps be integrated in the nonlinear crystal as in [41,42]. A polarization rotation analysis of the fundamental cavity beam for the case of intracavity SHG and Q-Switching in QPM, can be found in [41]. The polarization rotation there discussed for the case of PPLN, sets a basis for polarization rotation without Q-Switching, by removing the intracavity Brewster plate the authors include. However, it would also affect the polarization of the IR external image in its passage through the PPLN crystal, so it is not obvious that it would become possible when rather than SHG, it is SFM with an external image that is aimed. In [42], an example for the case of Type II BPM SHG in KTP is provided. In trying to integrate the Pockels cell in the nonlinear crystal, a scheme must be identified, based on a suitable nonlinear crystal, where the fast and slow axes do not rotate with the applied field as in [41,42].

There are still issues to be investigated in order to minimize the effect of relaxation oscillations on the shortest gating time achievable. There is, however, a reasonable basis for overcoming or strongly mitigating this problem, based on a scheme such as that in Fig. 10(c). In the meantime,

Optics EXPRESS

there are existing feedback and pre-compensation techniques referenced in the text to address this problem.

## Funding

Government of Spain, Ministerio de Ciencia, Innovación y Universidades (TEC2017-88899-C2-1-R); European Regional Development Fund.

## Disclosures

The authors declare that there are no conflicts of interest related to this article.

## References

1. O. David, N. S. Kopeika, and B. Weizer, "Range gated active night vision system for automobiles," Appl. Opt. **45**(28), 7248–7254 (2006).
2. M. Laurenzis, F. Christnacher, and D. Monnin, "Long-range three-dimensional active imaging with superresolution depth mapping," Opt. Lett. **32**(21), 3146–3148 (2007).
3. See for example ON SEMICONDUCTOR KAE-02150 EMCCD sensor at https://www.onsemi.com/pub/Collateral/KAE02150-D.PDF.
4. E. Repasi, P. Lutzmann, O. Steinvall, M. Elmqvist, B. Göhler, and G. Anstett, "Advanced short-wavelength infrared range-gated imaging for ground applications in monostatic and bistatic configuration," Appl. Opt. **48**(31), 5956–5969 (2009).
5. There is in fact an electron bombardment image intensifier tube developed by INTEVAC Inc., based on an InGaAs photocathode that operates in the SWIR up to 1.6 μm. It is of very restricted availability, and has not been considered in this work, aimed at a widespread potential use. (https://www.intevac.com/intevacphotonics/livar-506/).
6. J. H. Taylor and H. W. Yates, "Atmospheric Transmission in the Infrared," J. Opt. Soc. Am. **47**(3), 223–226 (1957).
7. J. E. Midwinter, "Image conversion from 1.6 μ to the visible in lithium niobate," Appl. Phys. Lett. **12**(3), 68–70 (1968).
8. C. Pedersen, E. Karamehmedović, J. S. Dam, and P. Tidemand-Lichtenberg, "Enhanced 2D-image upconversion using solid-state lasers," Opt. Express **17**(23), 20885–20890 (2009).
9. A. J. Torregrosa, H. Maestre, and J. Capmany, "Intra-cavity upconversion to 631 nm of images illuminated by an eye-safe ASE source at 1550 nm," Opt. Lett. **40**(22), 5315–5318 (2015).
10. R. Demur, R. Garioud, A. Grisard, E. Lallier, L. Leviandier, L. Morvan, N. Treps, and C. Fabre, "Near-infrared to visible upconversion imaging using a broadband pump laser," Opt. Express **26**(10), 13252–13263 (2018).
11. J. S. Dam, P. Tidemand-Lichtenberg, and C. Pedersen, "Room-temperature mid-infrared single-photon spectral imaging," Nat. Photonics **6**(11), 788–793 (2012).
12. A. J. Torregrosa, H. Maestre, M. L. Rico, and J. Capmany, "Compact self-illuminated image upconversion system based on intracavity second-harmonic generation," Opt. Lett. **43**(20), 5050–5053 (2018).
13. S. Junaid, J. Tomko, M. P. Semtsiv, J. Kischkat, W. T. Masselink, C. Pedersen, and P. Tidemand-Lichtenberg, "Mid-infrared upconversion based hyperspectral imaging," Opt. Express **26**(3), 2203–2211 (2018).
14. Y. P. Tseng, P. Bouzy, C. Pedersen, N. Stone, and P. Tidemand-Lichtenberg, "Upconversion raster scanning microscope for long-wavelength infrared imaging of breast cancer .microcalcifications," Biomed. Opt. Express **9**(10), 4979–4987 (2018).
15. S. Fan, F. Qi, T. Notake, K. Nawata, Y. Takida, T. Matsukawa, and H. Minamide, "Diffraction-limited real-time terahertz imaging by optical frequency up-conversion in a DAST crystal," Opt. Express **23**(6), 7611–7618 (2015).
16. J. E. Midwinter, "Parametric Infrared Image Converters," IEEE J. Quantum Electron. **4**(11), 716–720 (1968).
17. J. W. Goodman, in *Introduction to Fourier Optics* (Roberts & Co., 2005).
18. G. D. Boyd and D. A. Kleinman, "Parametric Interaction of Focused Gaussian Light Beams," J. Appl. Phys. **39**(8), 3597–3639 (1968).
19. R. G. Smith, "Theory of intracavity optical second-harmoinc generation," IEEE J. Quantum Electron. **6**(4), 215–223 (1970).
20. J. E. Geusic, H. J. Levinstein, S. Singh, R. G. Smith, and L. G. Van Utert, "Continuous 0.532 μ solid-state source using $Ba_2NaNb_5O_{15}$," Appl. Phys. Lett. **12**(9), 306–308 (1968).
21. M. Born and E. Wolf, in *Principles of Optics:Electromagnetic Theory of Propagation, Interference and Diffraction of Light*, 6th Edition, (Pergamon, 1993).
22. Z. Song, L. Liub, Y. Zhoub, D. Liub, and H. Renb, "Electro-optic modulation of light propagating near the optic axis with any polarization in uniaxial crystals," Optik **117**(9), 418–422 (2006).
23. R. C. Eckardt, H. Masuda, Y. X. Fan, and R. L. Byer, "Absolute and relative nonlinear optical coefficients of KDP, KD*P, $BaB_2O_4$, $LiIO_3$, MgO:LiNb $O_3$, and KTP measured by phase-matched second-harmonic generation," IEEE J. Quantum Electron. **26**(5), 922–933 (1990).
24. Z. Chen, B. Liu, S. Wang, and E. Liu, "Polarization-modulated three-dimensional imaging using a large-aperture electro-optic modulator," Appl. Opt. **57**(27), 7750–7756 (2018).

Optics EXPRESS


25. J. Warner, "Phase-Matching for Optical Up-Conversion with Maximum Angular Aperture-Theory and Practice," Opt. Quantum Electron. **1**(1), 25–28 (1969).
26. H. Maestre, A. J. Torregrosa, C. R. Fernández-Pousa, and J. Capmany, "IR-to-visible image upconverter under nonlinear crystal thermal gradient operation," Opt. Express **26**(2), 1133–1144 (2018).
27. H. Suchowski, B. D. Bruner, A. Arie, and Y. Silberberg, "Broadband frequency conversion," Opt. Photonics News **21**(10), 36–41 (2010).
28. Y. R. Shen, in *The Principles of Nonlinear Optics*, (Wiley, 1984).
29. PPST free software from St. Andrews University, Scotland, available at: https://www.st-andrews.ac.uk/~psst/
30. L. Friob, P. Mandel, and E. A. Viktorov, "Intracavity second harmonic generation in a Fabry–Perot resonator: I. Polarization effects," Quantum Semiclassical Opt. **10**(1), 1–17 (1998).
31. A. E. Siegman, *Lasers*, (Universiy Science Books, 1896).
32. Otsuka in *Nonlinear Dynamics in Optical Complex Systems*. Series: Advances in Opto-Electronics (Kluwer, 1999). Also, (Springer, 2000).
33. T. Baer, "Large-amplitude fluctuations due to longitudinal mode coupling in diode-pumped intracavity-doubled Nd:YAG lasers," J. Opt. Soc. Am. B **3**(9), 1175–1180 (1986).
34. G. P. Agrawal, in *Fiber-Optic Communication Systems, Third Edition* (Wiley, 2002).
35. A. V. Smith, SNLO software AS-Photonics, free download available at: http://www.as-photonics.com/snlo.
36. P. P. Yaney and L. G. DeShazer, "Spectroscopic studies and analysis of the laser states of $Nd^{3+}$ in $YVO_4$," J. Opt. Soc. Am. B **66**(12), 1405–1414 (1976).
37. C. Larsen, D. Noordegraaf, P. M. W. Skovgaard, K. P. Hansen, K. E. Mattsson, and O. Bang, "Gain-switched CW fiber laser for improved supercontinuum generation in a PCF," Opt. Express **19**(16), 14883–14891 (2011).
38. T. J. Kane, "Intensity-Noise in Diode-Pumped Single-Frequency Nd:YAG Lasers and its Control by Electronic Feedback," IEEE Photonics Technol. Lett. **2**(4), 244–245 (1990).
39. N. Dokhane and G. L. Lippi, "Improved direct modulation technique for faster switching of diode lasers," IEE Proc.: Optoelectron. **149**(1), 7–16 (2002).
40. J. Zondy, M. Abed, and S. Khodja, "Twin-crystal walk-off-compensated type-II second-harmonic generation: single-pass and cavity-enhanced experiments in $KTiOPO_4$," J. Opt. Soc. Am. B **11**(12), 2368–2379 (1994).
41. Y. H. Chen, Y. C. Huang, Y. Y. Lin, and Y. F. Chen, "Intracavity PPLN crystals for ultra-low-voltage laser Q-switching and high-efficiency wavelength conversion," Appl. Phys. B **80**(7), 889–896 (2005).
42. T. Taira, "Q-Switching and Frequency Doubling of Solid-state Lasers by a Single Intracavity KTP Crystal," IEEE J. Quantum Electron. **30**(3), 800–804 (1994).